AGU PUBLICATIONS

Geophysical Research Letters

RESEARCH LETTER
10.1002/2015GL066463

Key Points:
- Anticyclonic eddies funnel marine particles into a wineglass shape to 1000 m, controlling export
- The slope of the wineglass, *R*, is the ratio of radial advection to particle sinking, such that particles are sorted by size
- *R* thus represents a tool to predict radial particle movement, here modeled as the residual ageostrophic velocity of the eddy

Supporting Information:
- Supporting Information S1

Correspondence to:
A. M. Waite,
Anya.Waite@awi.de

Citation:
Waite, A. M., L. Stemmann, L. Guidi, P. H. R. Calil, A. M. C. Hogg, M. Feng, P. A. Thompson, M. Picheral, and G. Gorsky (2016), The wineglass effect shapes particle export to the deep ocean in mesoscale eddies, *Geophys. Res. Lett.*, *43*, 9791–9800, doi:10.1002/2015GL066463.

Received 5 OCT 2015
Accepted 29 AUG 2016
Accepted article online 31 AUG 2016
Published online 19 SEP 2016

©2016. The Authors.
This is an open access article under the terms of the Creative Commons Attribution-NonCommercial-NoDerivs License, which permits use and distribution in any medium, provided the original work is properly cited, the use is non-commercial and no modifications or adaptations are made.

The wineglass effect shapes particle export to the deep ocean in mesoscale eddies

Anya M. Waite[1,2,3], Lars Stemmann[4], Lionel Guidi[4,5], Paulo H. R. Calil[6], Andrew Mc C. Hogg[7], Ming Feng[8], Peter A. Thompson[9], Marc Picheral[4,6], and Gaby Gorsky[4]

[1]Oceans Institute and School of Environmental Systems Engineering, University of Western Australia, Crawley, Western Australia, Australia, [2]Now at Alfred Wegener Institute Helmholz Centre for Polar and Marine Research, Bremerhaven, Germany, [3]Now at Universität Bremen, Fachbereich 2 Biology/Chemistry, Bremen, Germany, [4]Sorbonne Universités, UPMC, Villefranche/mer, France, [5]Centre National de la Recherche Scientifique, Villefranche-sur-Mer, France, [6]Laboratório de Dinâmica e Modelagem Oceânica (DinaMO), Instituto de Oceanografia, Universidade Federal do Rio Grande, Rio Grande, Brazil, [7]Research School of Earth Sciences, Australian National University, Canberra, Australian Capital Territory, Australia, [8]Commonwealth Scientific and Industrial Research Organization Marine and Atmospheric Research, Floreat, Western Australia, Australia, [9]Commonwealth Scientific and Industrial Research Organization Marine and Atmospheric Research, Hobart, Tasmania, Australia

Abstract Mesoscale eddies in the ocean strongly impact the distribution of planktonic particles, mediating carbon fluxes over ~1/3 of the world ocean. However, mechanisms controlling particle transport through eddies are complex and challenging to measure in situ. Here we show the subsurface distribution of eddy particles funneled into a wineglass shape down to 1000 m, leading to a sevenfold increase of vertical carbon flux in the eddy center versus the eddy flanks, the "wineglass effect". We show that the slope of the wineglass (*R*) is the ratio of particle sinking velocity to the radially inward velocity, such that *R* represents a tool to predict radial particle movement (here 0.05 m s^{-1}). A simple model of eddy spindown predicts such an ageostrophic flow concentrating particles in the eddy center. We explore how size-specific particle flux toward the eddy center impacts eddies' biogeochemistry and export fluxes.

1. Introduction

Mesoscale eddies drive the periodic enhancement of vertical organic carbon export to the mesopelagic through localized increases in primary production [*Levy et al.*, 1998] and by enhanced vertical velocities associated with eddy perimeters and fronts [*Van Haren et al.*, 2006]. However, at present there is a wide range of proposed mechanisms and little consensus on the precise pathways by which eddies control particulate organic carbon (POC) export within the eddies themselves. Cyclones in the tropical Atlantic increased POC fluxes by 2–4 times [*Alonso-Gonzalez et al.*, 2013], with zooplankton downward migration playing an important role. Cyclones can trigger high local subsurface respiration rates via the production of surface organic matter [*Mourino-Carballido and Anderson*, 2009]. Elsewhere, cyclones have been seen to be dominated by local effects with no net enhancement of vertical flux [*Benitez-Nelson and McGillicuddy*, 2008].

An early model by Franks and coworkers [*Franks et al.*, 1986] suggested that anticyclones could enhance productivity over the time scale of eddy relaxation (60 days) through upward movement of the pycnocline. However, the small number of papers sampling anticyclones (quite sparsely) in the field has suggested that they suppress productivity locally because of their deeper mixed layer depth [*Hansen et al.*, 2010; *Moutin and Prieur*, 2012]. Anticyclones carrying water trapped from productive coasts move this water into oligotrophic gyres, enhancing productivity locally [*Ladd et al.*, 2009; *Waite et al.*, 2016]. Recent work suggests that at the perimeter of anticyclones, subduction of productive waters along isopycnals drives the export of both large and small POC well below the euphotic zone, along density interfaces [*Samuelsen et al.*, 2012; *Omand et al.*, 2015; *Waite et al.*, 2016]. On a seasonal time scale, mixed-layer deepening has been implicated in fueling the continued productivity of anticyclones in oligotrophic gyres [*Dufois et al.*, 2016].

The impact of anticyclone submesoscale circulation on particle flux was considered in more detail by *Zhou and coworkers* [2013] who used ^{234}Th-based measurements and a conceptual model to show theoretically that anticyclones could increase vertical flux by gentle inward surface transport toward the eddy center (on the order of 0.01 m s^{-1}), though they conclude that the center of the eddy is likely to have a low flux. These authors point out that direct measurements of POC in mesoscale eddies at high spatial resolution

are rare, as is the resolution of submesoscale motions outside of eddy margins. Radial particle transport was also predicted in a model by *Samuelsen et al.* [2012], who showed surface particle trajectories radially outward (the opposite direction than that shown by *Zhou and coworkers* [2013]). Particles' vertical transit pathways as they sink downward through eddies remain largely unresolved, and how they contribute to vertical export and carbon sequestration processes, both within eddies and in the context of broader global carbon flux patterns, is not fully understood.

For two anticyclonic mesoscale eddies, we present detailed field measurements showing the funneling of particles below the euphotic zone into a subsurface wineglass shape down to 1000 m. We demonstrate that there exists a subsurface slope in particle distributions that is steeper than the eddy isopycnals and that this slope increases with particle size. This suggests that particle distribution is not driven purely by isopycnal motion and that both particle sinking rates (which generally increase with particle size) and radial motions should govern their distributions. We test our hypothesis (1) via direct estimation of the radial velocity and (2) via a very simple first-order model.

2. Field Observations

Were executed at sea, transecting two mesoscale anticyclonic eddies: first, an eddy of the southward flowing Leeuwin Current (LC), sampled from the R/V *Southern Surveyor* in May 2006 in the eastern Indian Ocean and, second, an eddy in the Mediterranean Sea (MS) sampled from the R/V *Atalante* in July 2008. The forming anticyclonic mesoscale eddy in the LC was a large (200 km in diameter, 1000 m deep) feature, whose horizontal velocities reached 1 m s^{-1} to a depth of 150 m, with strong vertical shear [*Paterson et al.*, 2008]. The MS eddy was of a similar size, 70 km in diameter and 800 m in depth. The MS eddy was oligotrophic but enriched in dissolved organic carbon compared to the surrounding water mass. Both were sampled to 1000 m.

For the LC eddy, we transected the full diameter of the eddy, profiling to 1000 m every 18.5 km (10 nm) along 113.6° E between 31.6° and 34°S (Figures 1a and 1b). For the MS eddy, we sampled the southern eddy radius at 5 stations on three half-transects toward the center of the eddy. (Figures 2a and 2b). Physical variables were measured with a Sea-Bird Electronics 9/1 dual-sensor conductivity-temperature-depth unit. For both eddies, particle size distributions (equivalent spherical diameter (ESD) >60 μm) were measured in situ along a cross-eddy transect using the Underwater Vision Profiler 4 (UVP4) in the LC eddy and the UVP5 in the MS eddy ([*Picheral et al.*, 2010]). To avoid light contamination, images deeper than 40 m were used for day profiles with the UVP4. Objects in each image were detected, sized, and enumerated on custom software [*Picheral et al.*, 2010] based on the lateral scattering of light from a particle. Total number of pixels was converted to equivalent spherical diameter (ESD). Vertical particle fluxes were calculated from ESD (as in *Guidi et al.* [2008]; see supporting information).

The UVP data revealed a wineglass-shaped subsurface particle distribution in the LC eddy, with greatest concentration of particles high up in the water column and a deep central plume of particles reaching to 1000 m depth (Figures 1c and 1d). Particularly interesting was the vertical segregation of small and large particles, with smaller particles having a shallower concentration maximum. Similar patterns were seen at lower spatial resolution in the MS eddy (Figures 2c and 2d). The sloping sides of the wineglass (i.e., the slope of particle concentration isolines relative to the isopycnals) were significantly steeper for large particles than for small particles (chi-square $P < 0.001$) in both LC and MS eddies (Table 1).

Earlier work on the LC eddy suggested particles entered the eddy from the coast along the $\rho = 25.5$ potential density contour [*Waite et al.*, 2016], resulting in the particle-rich layer between 200 and 300 m in the eddy center. The LC eddy had particle concentrations (approximately 400 particles L^{-1}) 10 times that of the MS eddy (approximately 40 particles L^{-1}), reflecting a difference in productivity between the two oligotrophic sites (very low in the Mediterranean sea (mean 0.02 mol C m^{-2} d^{-1} [*Psarra et al.*, 2000]) and higher in the LC eddy (0.1 mol C m^{-2} d^{-1} [*Waite et al.*, 2016]).

3. Mechanisms

We initially investigated, and rejected, two possible mechanisms likely to drive such particle distributions: (1) Downward vertical velocities within the eddy core and (2) shear-driven or turbulence-driven aggregation within the eddy core driving increased particle size and thus increased sedimentation rates in the eddy

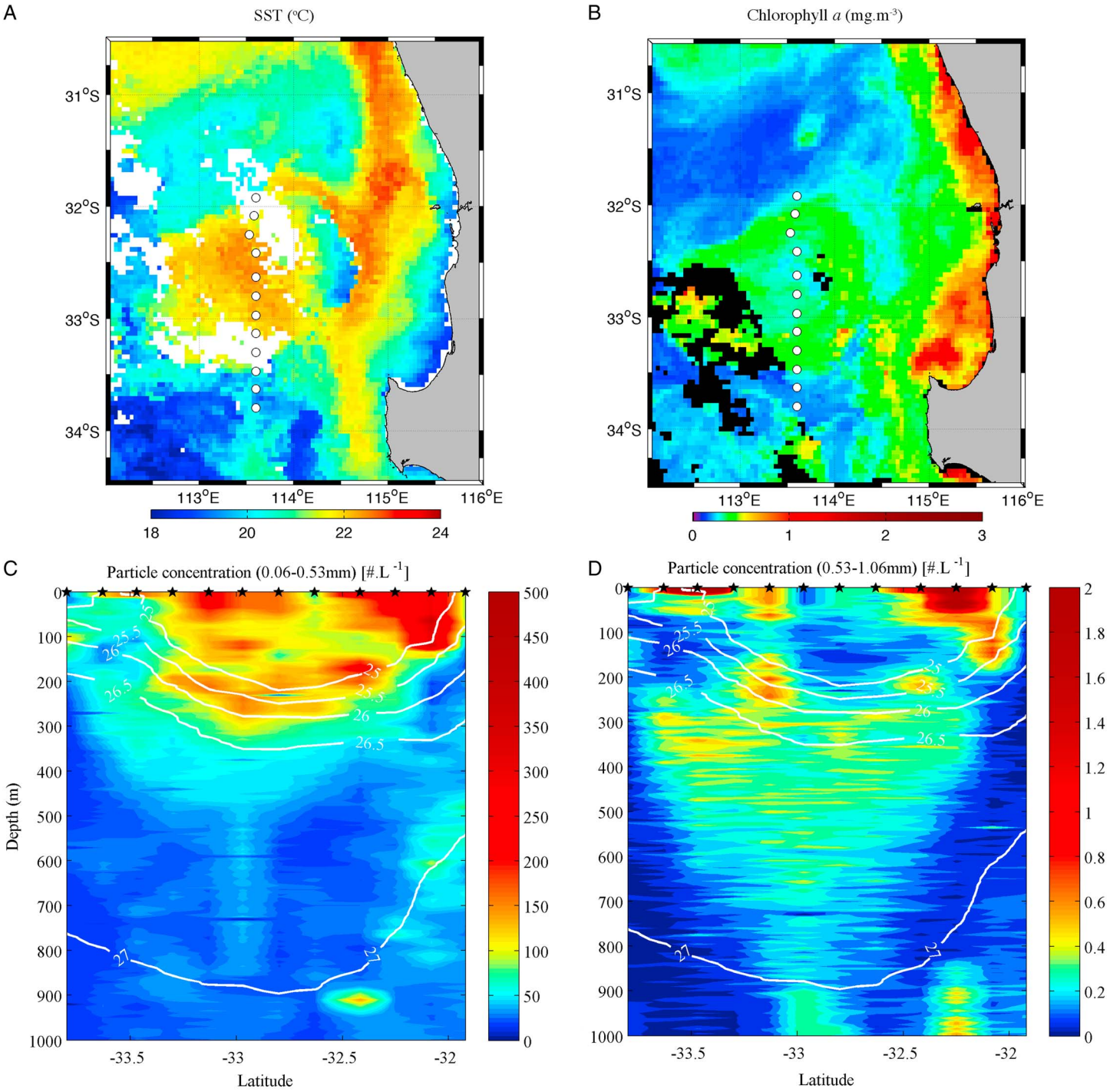

Figure 1. (a) Sea-surface temperature (°C) and (b) chlorophyll *a* (mg m^{-3}) derived from Moderate Resolution Imaging Spectroradiometer (MODIS) satellite, showing the mesoscale eddy in the Leeuwin Current (LC) off Australia. White circles indicate stations sampled. Spatial distributions of particles across the eddy: (c) Small (0.06–0.5 mm) and (d) large (0.5–1 mm) particles as measured by the Underwater Vision Profiler (UVP) shown in color, with isopycnals contoured in white.

center. For (1), we showed that vertical velocities [*Gomis et al.*, 2001] were not adequate in scale, or appropriate in distribution, to account for the particle distributions, since highest vertical velocities occurred at the eddy perimeter [*Paterson et al.*, 2008].

For (2), we evaluated the possible impact of shear-driven aggregation within the eddy core driving increased particle sedimentation rates in the eddy center using a coagulation model [*Jackson et al.*, 2005; *Jackson and*

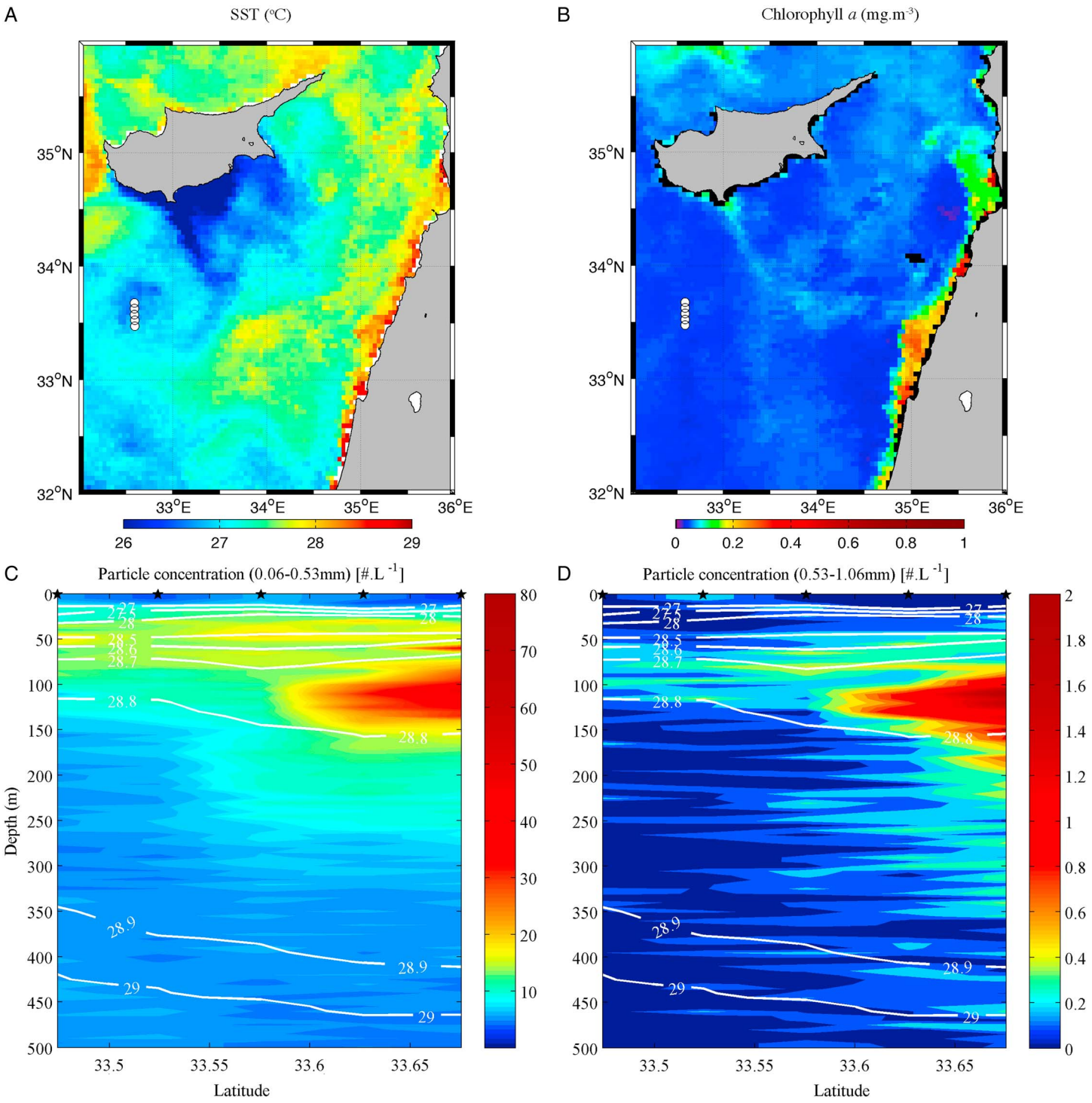

Figure 2. (a) Sea-surface temperature (°C) and (b) chlorophyll *a* (mg m^{-3}) derived from Moderate Resolution Imaging Spectroradiometer (MODIS) satellite, showing the mesoscale eddy sampled in the Mediterranean Sea (MS). White circles indicate stations sampled. Particle spatial distributions across the southern radius of the MS eddy as measured by the Underwater Vision Profiler (UVP) are shown with depth: (c) Small (0.06–0.5 mm) and (d) large (0.5–1 mm) with isopycnals contoured in white.

Lochmann, 1992]. Increases in particle contact rates can drive aggregation to a first order, while concentration (C) increases are more important (aggregation is proportional to C^2) [*Jackson*, 2001]. We assumed an individual particle size of 10 μm, a fractal dimension of 2.3, and an excess density of 0.01 g cm^{-3}. Calculations of coagulation rates used the "fractal" kernels, midway between the rectilinear and curvilinear kernels

Table 1. Scaling of the Wineglass Effect to Calculate the Radial Velocity Generating the Wineglass Shape[a]

Particle Category	Particle Size (mm)	Sinking Rate, s ($m\,d^{-1}$)	Measured Particle Slope, R (‰)	Radial Velocity, u ($m\,s^{-1}$)	Eddy-Specific Normalized Slope, Rt
			Leeuwin Current Eddy (LC)		
Small	0.06–0.5	~10	0.8 ± 0.5	~0.01–0.08	0.75
Medium	0.5–1	~50	0.8 ± 0.5	~0.03–0.08	0.3–8
Large	1–2	~100	3 ± 1.5	~0.07	12
			Mediterranean Eddy (MS)		
Small	0.06–0.5	~10	0.1 ± 0.5	~0.03	0.75
Med	0.5–1	~50	0.3 ± 0.5	~0.03–0.08	0.3–8
Large	1–2	~100	1.2 ± 1.5	~0.07	12

[a]Particle sizes were measured with an Underwater Vision Profiler (UVP), sinking rate s was assumed, and the slope R was measured as the difference in slope (in m/km) of particle concentration isolines against isopycnals. The isopycnal slopes were ($1.3 \pm 0.3\ m\,km^{-1}$) and ($6.8 \pm 1.6\ m\,km^{-1}$) in the LC and MS eddies, respectively The radial velocity u was triangulated from s and R. R_t = [s/(pycnocline depth)]/[u/eddy radius], normalizing R ($km\,m^{-1}$) to relevant length scales of individual eddies; here the Rossby Radius (50 km) is in the horizontal, and the depth of the pycnocline (200 m) is in the vertical.

[*Jackson*, 2001]. Coagulation both adds and subtracts mass for particles in a given size range. We calculated the instantaneous rates of particle gain and loss using the sectional representation of the particle size distribution at five depths (175, 250, 300, 350, and 400 m) as in *Stemmann et al.* [2004b] (supporting information). At shear rates from shipboard Acoustic Doppler Current Profiler (ADCP) data ($<0.01\ s^{-1}$), the impact of coagulation by shear on the size spectra was negligible for all size classes (minimum 100 μm) ($1/Q_i\,dQ_i/dt < 0.008\ d^{-1}$, where Q_i is particle biovolume).

3.1. Our Hypothesis

We hypothesized that the slope in the concentration isolines would represent the net effect of the downward sinking vector set by the settling velocity and the radial vector toward the eddy center (or away from the eddy center above the pycnocline). Since settling velocity is generally believed to increase with particle size, this would account for the change in slope as particle size increases. As they sink through the pycnocline to denser water, all particles' sinking rates decrease, so particles spend more time in the lower pycnocline than they do in the upper pycnocline. If the lower pycnocline has a gentle radially inward velocity, particles will be moved toward the eddy center there. Slower sinking particles with a longer residence time would be more affected than larger, faster sinking particles and would therefore be more concentrated at the eddy center, with the slopes of their concentration isolines flatter (Figures 1c, 11d, 2c, and 2d). This phenomenon, which we call "the wineglass effect," would explain particle sorting process we observed.

Because the median sinking rate for a given particle size is reasonably well constrained (albeit with a very large variance) [*Guidi et al.*, 2008], for large particle sample sizes we should be able to use the particle slope to back calculate the radial velocity that generated it.

The wineglass slope R was directly measured, as a percent deviation from the isopycnal for each particle size class of interest (here 60 μm–500 μm, 500 μm–1 mm, and > 1 mm). The slope of the concentration isolines for each size class was then hypothesized to be a function of (vertical) sinking rate (s) and (horizontal) radial velocity (u) (Table 1). Our measurements of R range from 0.1 to > 3 (Figures 1 and 2 and Table 1), and the estimated radially inward velocity needed to generate these slopes range from 0.01 to $0.08\ m\,s^{-1}$.

4. Modeling

Having estimated the radial velocities u needed to produce the observed slopes, we sought a physical mechanism that might drive velocities of this scale. To first order, radial ageostrophic velocities due to frictional spindown of the eddy will bring isopycnals back to their equilibrium depths. This will generate inward velocities below the pycnocline and outward velocities above the pycnocline. The former will shape the wineglass by concentrating particles in the central portion of anticyclones as they sink through the pycnocline. *Franks et al.* [1986] used a similar model to explain biological production within the cores of anticyclones, via vertical nutrient transfer within the eddy. In the case of the wineglass effect, we explore how the horizontal component will tilt the trajectory of sinking particles, concentrating them toward the eddy center.

This simple model for eddy particle motion assumed (1) that the primary mode of vertical movement of particles is due to settling, (2) that particle settling velocities depend linearly upon the density difference between the particles and the local water density and that particle settling rate increases with particle size r with a range of possibly exponents described in the literature ($r^{0.5} - r^{1.3}$) [*Guidi et al.*, 2009; *Waite et al.*, 1997], and (3) that horizontal motion can be decomposed into a geostrophic component (around the vortex) and an ageostrophic radial component. The ageostrophic velocities were assumed to be driven by turbulent Reynolds stress within the water column, parameterized via a constant anisotropic eddy diffusivity.

4.1. Model Setup

We assumed a rotationally symmetric eddy with cylindrical polar coordinates (origin at eddy center, and radial and vertical coordinates are r and z, respectively). We assume that centrifugal forces within the eddy are negligible compared with gravitational acceleration and that the large scale structure of the eddy is stable [*Kriest et al.*, 2012] with respect to further shear instability or baroclinic instability. The eddy can then be defined by the geostrophic velocity v_g in the tangential direction (defined positive anticlockwise) that is in balance with the Coriolis force as given by the thermal wind equation [*Killworth*, 1980],

$$f\frac{\partial v_g}{\partial z} = \frac{-g}{\rho_0}\frac{\partial \rho}{\partial r} \tag{1}$$

where f is the Coriolis parameter, g is the acceleration due to gravity, ρ the local fluid density, and ρ_0 is the minimum density at $r = z = 0$. We can write a friction-Coriolis balance within our eddy as (neglecting the centrifugal forcing)

$$fu = K_h\left(\frac{\partial^2 v_g}{\partial r^2} + \frac{1}{r}\frac{\partial v_g}{\partial r} - \frac{v_g}{r^2}\right) + K_v\frac{\partial^2 v_g}{\partial z^2} \tag{2}$$

where u is the ageostrophic velocity in the radial direction (defined as being positive outward), K_h is the horizontal eddy viscosity, and K_v the vertical eddy viscosity. The model thus includes both the interfacial Ekman effect due to vertical friction [*Vallis*, 2006] and horizontal friction [*Csanady*, 1979], but it can be shown that it is the former effect which governs radial velocity, while the latter controls spindown effects. Substitute (1) into (2) to give

$$\frac{\partial u}{\partial z} = \frac{-g}{f^2\rho_0}\left[K_h\left(\frac{\partial^3 \rho}{\partial r^3} + \frac{1}{r}\frac{\partial^2 \rho}{\partial r^2} - \frac{1}{r^2}\frac{\partial \rho}{\partial r}\right) + K_v\frac{\partial^3 \rho}{\partial z^2 \partial r}\right] \tag{3}$$

This equation describes a velocity which is radially outward above the pycnocline and radially inward below the pycnocline (Figure 3a). The velocity acts to transport water along isopcynals and would therefore be associated a small vertical component (w). Advection along isopycnals implies that the vertical velocity can be obtained from the horizontal velocity and the isopycnal slope:

$$w = -u\left(\frac{\partial \rho}{\partial r} \Big/ \frac{\partial \rho}{\partial z}\right) \tag{4}$$

We assume that the sinking velocities will depend upon local water density, so we write

$$s = s_0\frac{\rho_p - \rho}{\rho_p - \rho_0} \tag{5}$$

where s_0 is the assumed known base sinking rate (when $\rho = \rho_0$) and ρ_p is the particle density. This equation describes a particle sinking rate that decreases as the particle passes through the pycnocline; particles will spend longer in the lower pycnocline where the velocity is toward the center of the eddy. The net effect is that particles will be closer to the eddy center after passing through the pycnocline. We use the velocity field u (by numerically integrating (3)) and w (4), along with sinking rate s (5) to trace particles from the interior of the eddy as they fall through the pycnocline. In this case, we assume $K_h = 10\,\mathrm{m^2\,s^{-1}}$, $K_v = 10^{-3}\,\mathrm{m^2\,s^{-1}}$, $f = 5 \times 10^{-7}\,\mathrm{s^{-1}}$, $\rho_p/\rho_0 = 1.003$ and use a density field with a 200 m thick pycnocline as shown by the grey contours (Figure 3a). For these parameters, we vary sinking rate s from 2 to 30 $\mathrm{m\,d^{-1}}$ to demonstrate the variation in the shape of the wineglass with sinking rate; parameters such as the eddy viscosity and density contrast govern the behavior of the model in a similar way.

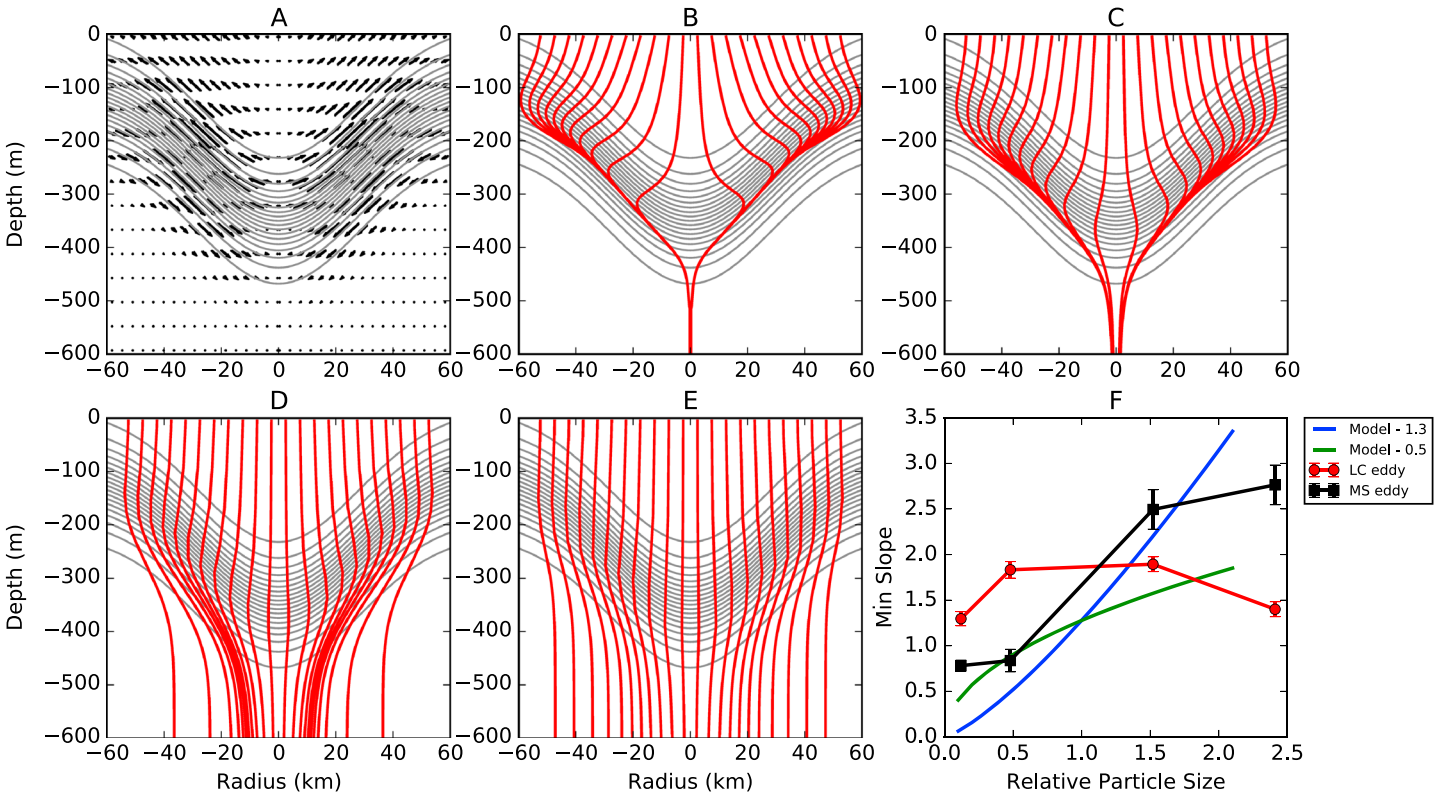

Figure 3. Particle trajectories plotted against ageostrophic velocity field for four cases with different base sinking rate: (a) The radial ageostrophic velocity field, (b) particle trajectories (red lines) for sinking rate of 2 m d^{-1}, (c) trajectories for sinking rate of 5 m d^{-1}, (d) trajectories for sinking rate of 15 m d^{-1}, and (e) trajectories for sinking rate of 30 m d^{-1}. Grey contours show the density field, which is assumed to be rotationally symmetric. (f) Raw comparison of wineglass shape indices between model and field data showing underlying process similarity without directly scaling the model. Predicted relationship between particle size and *R* generated by sinking particles of that size (blue), with observed statistically significant increase of wineglass slope with particle size from LC and MS eddies. Model values are given for the case where sinking rate is proportional to particle radius as $r^{1.3}$ and $r^{0.5}$, which covers the range of measured literature values (see text).

4.2. Model Output

The measure of the wineglass shape can be given by the ratio *R* between ageostrophic radial velocity and sinking rate. When *R* becomes small, the wineglass shape is more pronounced, as shown in Figures 3b and 3c (versus Figures 3d and 3e). The friction-Coriolis balance obtained by *Flierl and Mied* [1985] is the solution used in this study. A simple particle tracking algorithm was implemented using the radial velocities and the vertical velocities plus the sinking rate in order to see if the obtained solution would yield a shape that is consistent with the wineglass; that is, as particles descend into the deep ocean they are slightly advected inward; hence, the funneling effect within the eddy is obtained. Particle trajectories were calculated from a given initial position in the upper water column subject to ageostrophic velocities and settling, based solely on a given density structure. The ageostrophic horizontal velocity field acted to disperse particles radially outward in the upper thermocline, while flow centerward occurred in the lower thermocline. The behavior of particles within the eddy was critically dependent on particle sinking rate and thus on particle size [*Waite et al.*, 1997; *Guidi et al.*, 2008]. Small, slower-sinking particles spent longer in the region where velocity was oriented toward the center of the eddy. So while all particles were closer to the eddy center after passing through the thermocline, smaller ones were more concentrated there, creating the vertical segregation of different particle size classes and the different size-specific slopes of the wineglass effect (Figures 3b–3e).

4.3. Comparison Between Model Output and Field Data

The slope of the wineglass (*R*) increases with increasing particle size, scaling similarly in the field data and in the model (Figure 3f) and supporting the proposed interaction between particle sinking rate and eddy velocities in governing the observed wineglass shape. The simplicity of the model does not make it suitable for direct comparison with in situ data: In the model we varied sinking rate from 2 to 30 m d^{-1} to demonstrate

the variation in the shape of the wineglass with relative sinking rate; these are 2–5 times lower than expected actual rates, though some large particles are known to sink slowly. There will be other processes that will affect both particle sinking and ageostrophic velocities, which are not explicitly resolved here. For example, eddy/wind interaction will generate upwelling within anticyclonic eddies [*Macintyre et al.*, 1995]. This will tend to maintain sinking particles for longer periods within the eddy core. Also, nonlinear frictional effects, which are known to generate large vertical velocities and convergence at the edges of mesoscale eddies will become important as the Rossby number tends to unity and the quasi-geostrophic assumption of the model is violated [*Martin and Richards*, 2001; *McGillicuddy et al.*, 2007]. This will be particularly true at the edges of mesoscale structures [*Mahadevan and Tandon*, 2006; *Mahadevan et al.*, 2008]. Adiabatic processes such as surface frontogenesis may also generate large vertical velocities in regions of intense gradients of density and relative vorticity. In general, these will also be larger at the edges of eddies [*Calil and Richards*, 2010]. The extent to which the wineglass effect is altered by these processes is unknown. However, if the flow is along isopycnals, accumulation of particulate material at the center of anticyclones will be favored as particles settle from the edges [*Omand et al.*, 2015].

5. Impacts and Other Considerations—Scaling *R* as *Rt*

Estimating R as a percent slope intrinsically compares sinking rate s with radial velocity u, where the latter is about 100 times greater. However, we can gain insight here by considering the more specific spatial scales involved in the transit of an individual particle through a mesoscale eddy. Normalizing both numerator and denominator to the specific length scales traveled in the generation of the wineglass effect, we normalize s to the pycnocline height H (here about 200 m) and u by the Rossby radius r_d (in this case about 50 km). We thus go from $R = s/u$ to a derived value Rt, the ratio of the number of vertical and horizontal eddy transits per day (in day^{-1}):

$$R_t = \frac{r_d}{H}\frac{S}{u}$$

R and Rt would have a constant ratio for a given mesoscale feature. Here, by definition, when $Rt \sim 1$, vertical and horizontal eddy transits per day (in day^{-1}) are of the same order, such that the wineglass effect has a visible impact on particles' sinking trajectory. However, note that the inverse of these numbers (in day^{-1}) is a time scale for a single eddy transit, τ (in days). We can therefore consider Rt equally as a ratio of time scales, or eddy residence times (in days), $\tau u/\tau s$ where τu is the time scale for a particle to transit the eddy radially and τs is the time scale to sink vertically through the pycnocline. Thus, we can use Rt in a manner analogous to a Damköhler number [see *Oldham et al.*, 2013] allowing Rt to take on a more specific and intuitive meaning: Rt, the normalized slope of the wineglass, is the ratio of time scales of the processes generating it.

This should help us predict impacts: If Rt is very low, the radial transport time scale is much shorter than the sinking time scale, particles are sinking slowly, and the probability of their being simply concentrated in the eddy center is increased (potentially the case for smallest particles; Figure 1a). If $Rt \gg 1$, the horizontal residence time scale is much longer than the sinking time scale, suggesting that the particles would transit rapidly through the eddy without significant concentration in the eddy center, i.e., no wineglass effect. If Rt is close to 1, then particles would have the greatest probability of forming a wineglass shape (potentially the case for larger particles; Figure 1b).

The potential for particles to contribute locally to biogeochemical processes concentrating in the eddy center should thus increase as Rt decreases. This could lead to higher mineralization rates in the eddy core at very low Rt. There is anecdotal evidence for this; the observed increase in oxygen deficit in the core of the LC eddy suggests respiration as high as 0.1 mol O_2 m^{-2} d^{-1} [*Waite et al.*, 2016]. A smaller oxygen depletion is also visible in the MS eddy, which also shows enhanced concentrations of dissolved organic matter, likely sourced from partial remineralization of small particles not proceeding to full oxidation under extreme oligotrophy [*Moutin and Prieur*, 2012]. Similar patterns are seen in other eddies [*Moutin et al.*, 2012].

Larger particles operating around $Rt \sim 1$ will also concentrate in the eddy center, but over a larger vertical distance, decreasing the probability for remineralization losses higher in the water column, and potentially resulting in aggregation in the eddy center driven by concentration increases. Concentration increases are the most important trigger of aggregation, which is one of the principal drivers of enhanced vertical fluxes.

We therefore tested the hypothesis that an increase in particles occurred in the eddy center that would support greater vertical particle fluxes: Increases in particle flux in the eddy center were calculated as the ratio between flux at km = 118 (eddy center) and flux at km = 210 (eddy margin). To account for parameter sensitivity of the particle flux estimates from particle size spectra, they were calculated using two parameterizations [*Guidi et al*., 2008; *Stemmann et al*., 2004b] and assuming a carbon to dry weight ratio of 0.4. The two estimates yield similar spatial patterns in the flux with a twofold to sevenfold increase in the eddy center compared to the surrounding stations of the eddy flank.

6. Conclusions

The biogeochemical impact of the wineglass effect will be dependent on individual eddy productivity and history, as well as the particle size spectrum. Where *Rt* is low, the concentration of (small) particles is likely to drive an acceleration of the biogeochemical rates within or near the pycnocline, possibly accelerating grazing [*Stemmann et al*., 2004a; *Guidi et al*., 2008] and remineralization [*Waite et al*., 2000; *Jackson and Checkley*, 2011]. Where *Rt* is closer to 1, physical focusing of (larger) particles in the eddy center would increase sedimentary fluxes there and aggregation (being concentration dependent) would further increase sedimentation, deeper in the water column. Such increases in sedimentary fluxes could fuel hot spots for mesopelagic organisms and benthic communities [*Waniek et al*., 2005; *Wei et al*., 2010] in up to 1/6 of the world ocean. Inconsistencies in global remineralization budgets [*Burd et al*., 2010] remind us of these budgets' vulnerability to uncertainties in sparsely sampled and poorly quantified processes at the mesoscale and submesoscale. Here we demonstrate the critical importance of understanding the interaction of particles of different sizes with physical processes at a fine spatial scales, which has the potential to impact a significant fraction of carbon fluxes across the global ocean.

Acknowledgments

We acknowledge helpful comments on the manuscript from W.-J. von Appen, G.A. Jackson, D. Griffin, and R.F.C. Mantoura. The work was supported by grants from the Australian Research Council (DP0663670 and DP 1093510) to AMW and coworkers. We acknowledge the support of the BOUM project for the MS sampling cruise. Discussions in Villefranche were supported by a Study Leave grant to AMW from the University of Western Australia. L.S., M.P., and G.G. acknowledge the CNRS and the University of Pierre and Marie Curie. L.S. was supported by the chair VISION from CNRS/UPMC. P.H.R.C. acknowledges support from CNPq (process: 307385/2013-2). A.M.H. was supported by an Australian Research Council Future Fellowship FT120100842. For all data associated with this work please contact the corresponding author A. Waite, anya.waite@awi.de.

References

Alonso-Gonzalez, I. J., Aristegui, J., Lee, C., Sanchez-Vidal, A., Calafat, A., Fabres, J., Sangra, P., and Mason, E. 2013, Carbon dynamics within cyclonic eddies: Insights from a biomarker study. *PLoS One*, *8*, e82447, doi:10.1371/journal.pone.0082447.

Benitez-Nelson, C. R., and D. J. McGillicuddy Jr. (2008), Mesoscale physical-biological-biogeochemical linkages in the open ocean: An introduction to the results of E-flux and EDDIES programs, *Deep Sea Res., Part II*, *55*, 1133–1138.

Burd, A. B., et al. (2010), Assessing the apparent imbalance between geochemical and biochemical indicators of meso- and bathypelagic biological activity: What the @$#! is wrong with present calculations of carbon budgets?, *Deep Sea Res., Part II*, *57*, 1557–1571.

Calil, P. H. R., and K. J. Richards (2010), Transient upwelling hot spots in the oligotrophic North Pacific, *J. Geophys. Res.*, *115*, C02003, doi:10.1029/2009JC005360.

Csanady, G. T. (1979), Birth and death of a warm core ring, *J. Geophys. Res.*, *84*, 777–780, doi:10.1029/JC084iC02p00777.

Dufois, F., N. J. Hardman-Mountford, J. Greenwood, A. J. Richardson, M. Feng, and R. J. Matear (2016), Anticyclonic eddies are more productive than cyclonic eddies in subtropical gyres because of winter mixing, *Sci. Adv.*, *2*, e1600282, doi:10.1126/sciadv.1600282.

Flierl, G. R., and R. P. Mied (1985), Frictionally induced circulations and spin down of a warm core ring, *J. Geophys. Res.*, *90*, 8917–8927.

Franks, P. J. S., J. S. Wroblewski, and G. R. Fierl (1986), Prediction of phytoplankton growth in response to the frictional decay of a warm-core ring, *J. Geophys. Res.*, *91*, 7603–7610, doi:10.1029/JC091iC06p07603.

Gomis, D., S. Ruiz, and M. A. Pedder (2001), Diagnostic analysis of the 3D ageostrophic circulation from a multivariate spatial interpolation of CTD and ADCP data, *Deep Sea Res., Part I*, *48*, 269–295.

Guidi, L., G. A. Jackson, L. Stemmann, J. C. Miquel, M. Picheral, and G. Gorsky (2008), Relationship between particle size distribution and flux in the mesopelagic zone, *Deep Sea Res., Part I*, *55*, 1364–1374.

Guidi, L., L. Stemmann, G. A. Jackson, F. Ibanez, H. Claustre, L. Legendre, M. Picheral, and G. Gorsky (2009), Effects of phytoplankton community on production, size and export of large aggregates: A world ocean analysis, *Limnol. Oceanogr.*, *54*(6), 1951–1963.

Hansen, C., E. Kvaleberg, and A. Samuelsen (2010), Anticyclonic eddies in the Norwegian Sea; their generation, evolution and impact on primary production, *Deep Sea Res., Part I*, *57*, 1079–1091.

Jackson, G. A. (2001), Effect of coagulation on a model planktonic food web, *Deep Sea Res., Part II*, *48*, 95–123.

Jackson, G. A., and D. M. Checkley (2011), Particle size distributions in the upper 100 m water column and their implications for animal feeding in the plankton, *Deep Sea Res., Part I*, *58*, 283–297.

Jackson, G. A., and S. E. Lochmann (1992), Effect of coagulation on nutrient and light limitation of an algal bloom, *Limnol. Oceanogr.*, *37*, 77–89.

Jackson, G. A., A. M. Waite, and P. W. Boyd (2005), Role of algal aggregation in vertical carbon export during SOIREE and in other low biomass environments, *Geophys. Res. Lett.*, *32*, L13607, doi:10.1029/2005GL023180.

Killworth, P. D. (1980), Barotropic and baroclinic instability in rotating stratified fluids, *Dyn. Atmos. Oceans*, *4*, 143–184.

Kriest, I., A. Oschlies, and S. Khatiwala (2012), Sensitivity analysis of simple global marine biogeochemical models, *Global Biogeochem. Cycles*, *26*, GB2029, doi:10.1029/2011GB004072.

Ladd, C., W. R. Crawford, C. E. Harpold, W. K. Johnson, N. B. Kachel, P. J. Stabeno, and F. Whitney (2009), A synoptic survey of young mesoscale eddies in the Eastern Gulf of Alaska, *Deep Sea Res. Part II-Topical Studies Oceanogr.*, *56*, 2460–2473.

Levy, M., L. Memery, and G. Madec (1998), The onset of a bloom after deep winter convection in the northwestern Mediterranean Sea: Mesoscale process study with a primitive equation model, *J. Mar. Syst.*, *16*, 7–21.

Macintyre, S., A. L. Alldredge, and C. C. Gotschalk (1995), Accumulation of marine snow at density discontinuities in the water column, *Limnol. Oceanogr.*, *40*, 449–468.

Mahadevan, A., and A. M. I. T. Tandon (2006), An analysis of mechanisms for submesoscale vertical motion at ocean fronts, *Ocean Modell.*, *14*, 241–256.
Mahadevan, A., L. N. Thomas, and A. Tandon (2008), Comment on "eddy/wind interactions stimulate extraordinary mid-ocean plankton blooms", *Science*, *320*, 448.
Martin, A. P., and K. J. Richards (2001), Mechanisms for vertical nutrient transport within a North Atlantic mesoscale eddy, *Deep Sea Res. Part II: Topical Studies Oceanogr.*, *48*, 757–773.
Mcgillicuddy, D. J., Jr., et al. (2007), Eddy/wind interactions stimulate extraordinary mid-ocean plankton blooms, *Science*, *316*, 1021–1026.
Mourino-Carballido, B., and L. A. Anderson (2009), Net community production of oxygen derived from in vitro and in situ 1-D modeling techniques in a cyclonic mesoscale eddy in the Sargasso Sea, *Biogeosciences*, *6*, 1799–1810.
Moutin, T., and L. Prieur (2012), Influence of anticyclonic eddies on the Biogeochemistry from the Oligotrophic to the Ultraoligotrophic Mediterranean (BOUM cruise), *Biogeosciences*, *9*, 3827–3855.
Moutin, T., F. Van Wambeke, and L. Prieur (2012), Introduction to the Biogeochemistry from the Oligotrophic to the Ultraoligotrophic Mediterranean (BOUM) experiment, *Biogeosciences*, *9*, 3817–3825.
Oldham, C. E., D. E. Farrow, and S. Pfeiffer (2013), A generalized Damk¨ohler number for classifying material processing in hydrological systems, *Hydrol. Earth Syst. Sci.*, *17*, 1133–1148.
Omand, M. M., E. A. D'asaro, C. M. Lee, M. J. Perry, N. Briggs, I. Cetinic, and A. Mahadevan (2015), Eddy-driven subduction exports particulate organic carbon from the spring bloom, *Science*, *348*, 222–225.
Paterson, H. L., M. Feng, A. M. Waite, D. Gomis, L. E. Beckley, D. Holliday, and P. A. Thompson (2008), Physical and chemical signatures of a developing anticyclonic eddy in the Leeuwin Current, eastern Indian Ocean, *J. Geophys. Res.*, *113*, C07049, doi:10.1029/2007JC004707.
Picheral, M., L. Guidi, L. Stemmann, D. M. Karl, G. Iddaoud, and G. Gorsky (2010), The Underwater Vision Profiler 5: An advanced instrument for high spatial resolution studies of particle size spectra and zooplankton, *Limnol. Oceanogr. Methods*, *8*, 462–473.
Psarra, S., A. Tselepides, and L. Ignatiades (2000), Primary productivity in the oligotrophic Cretan Sea (NE Mediterranean): Seasonal and interannual variability, *Prog. Oceanogr.*, *46*, 187–204.
Samuelsen, S., S. Hjollo, J. A. Johannessen, and R. Patel (2012), Particle aggregation in anticyclonic eddies and implications for distribution of biomass, *Ocean Sci.*, *8*, 389–400.
Stemmann, L., G. A. Jackson, and G. Gorsky (2004a), A vertical model of particle size distributions and fluxes in the midwater column that includes biological and physical processes—Part II: Application to a three year survey in the NW Mediterranean Sea, *Deep Sea Res. Part I-Oceanogr. Res. Pap.*, *51*, 885–908.
Stemmann, L., G. A. Jackson, and G. Gorsky (2004b), A vertical model of particle size distributions and fluxes in the midwater column that includes biological and physical processes—Part II: Application to a three year survey in the NW Mediterranean Sea, *Deep Sea Res., Part I*, *51*, 885–908.
Vallis, G. K. (2006), *Atmospheric and Oceanic Fluid Dynamics: Fundamentals and Large-Scale Circulation*, Cambridge Univ. Press, Cambridge, U. K.
Van Haren, H., C. Millot, and I. Taupier-Letage (2006), Fast deep sinking in Mediterranean eddies, *Geophys. Res. Lett.*, 33, L04606, doi:10.1029/2005GL025367.
Waite, A. M., K. A. Safi, J. A. Hall, and S. D. Nodder (2000), Mass sedimentation of picoplankton embedded in organic aggregates, *Limnol. Oceanogr.*, *45*, 87–97.
Waite, A. M., L. E. Beckley, L. Guidi, J. P. Landrum, D. Holliday, J. Montoya, H. Paterson, M. Feng, P. A. Thompson, and E. J. Raes (2016), Cross-shelf transport, oxygen depletion, and nitrate release within a forming mesoscale eddy in the eastern Indian Ocean, *Limnol. Oceanogr.*, *61*(1), 103–121.
Waite, A., A. Fisher, P. A. Thompson, and P. J. Harrison (1997), Sinking rate versus cell volume relationships illuminate sinking rate control mechanisms in marine diatoms, *Mar. Ecol. Prog. Ser.*, *157*, 97–108.
Waniek, J. J., D. E. Schulz-Bull, T. Blanz, R. D. Prien, A. Oschlies, and T. J. Muller (2005), Interannual variability of deep water particle flux in relation to production and lateral sources in the northeast Atlantic, *Deep Sea Res., Part I*, *52*, 33–50.
Wei, C. L., et al. (2010), Global patterns and predictions of seafloor biomass using random forests, *PLoS One*, *5*, doi:10.1371/journal.pone.0015323.
Zhou, K., M. Dai, S. Kao, L. Wang, P. Xoi, F. Chai, J. Tian, and Y. Liu (2013), Apparent enhancement of ^{234}Th-based particle export associated with anticyclonic eddies, *Earth Planet. Sci. Lett.*, *381*, 198–209.